UNIVERSITY OF BATH

University of Bath

GTP-14-1417

USE OF PRESSURE MEASUREMENTS TO DETERMINE EFFECTIVENESS OF TURBINE RIM SEALS

J Michael Owen[1] **Kang Wu**[2] **James A Scobie**[1]

Carl M Sangan[1] **GeonHwan Cho**[1] **Gary D Lock**[1]

[1] Mechanical Engineering
University of Bath
Bath, BA2 7AY
United Kingdom

[2] Tsinghua University.
Thermal Engineering
Beijing, 100084
P.R. China

Corresponding author's email: c.m.sangan@bath.ac.uk

ABSTRACT

The ingress of hot gas through the rim seal of a gas turbine depends on the pressure difference between the mainstream flow in the turbine annulus and that in the wheel-space radially inward of the rim seal. In this paper, a previously published orifice model is modified so that the sealing effectiveness ε_c determined from concentration measurements in a rig could be used to determine ε_p the effectiveness determined from pressure measurements in an engine. It is assumed that there is a hypothetical 'sweet spot' on the vane platform where the measured pressures would ensure that the calculated value of ε_p equals ε_c, the value determined from concentration measurements. Experimental measurements for a radial-clearance seal show that, as predicted, the hypothetical pressure difference at the sweet spot is linearly related to the pressure difference measured at an arbitrary location on the vane platform. There is good agreement between the values of ε_p determined using the theoretical model and values of ε_c determined from concentration measurements. Supporting computations, using a 3D steady CFD code, show that the axial location of the sweet spot is very close to the upstream edge of the seal clearance. It is shown how parameters obtained from measurements of pressure and concentration in a rig could, in principle, be used to calculate the sealing effectiveness in an engine.

Nomenclature

b	radius of seal
B, C	constants
c	concentration of tracer gas
$C_{d,e}, C_{d,i}$	discharge coefficients for egress, ingress
C_F	flow coefficient
C_p	pressure coefficient $(= (p_2 - \bar{p}_2)/0.5\rho\Omega^2 b^2)$
$C_{w,o}$	nondimensional sealing flow rate $= (m/\mu b)$
g	normalized pressure difference across seal clearance $(=(p_1 - p_{2,min})/\Delta p)$
g^*	value of g when $C_{w,o} = 0$
$\hat{g}$	value of g to ensure $\varepsilon_p = \varepsilon_c$
G_c	seal-clearance ratio $(= s_c / b)$
m	mass flow rate
p	static pressure
$\bar{p}$	mean pressure
r	radius

Re_w	axial Reynolds number in annulus ($= \rho W b / \mu$)
Re_ϕ	rotational Reynolds number ($= \rho \Omega b^2 / \mu$)
s_c	seal clearance
U	bulk-mean average of sealing air in seal clearance
W	axial velocity in annulus
x	nondimensional axial distance in annulus ($= 2z/s_c$)
$\hat{x}$	value of x to ensure $\varepsilon_p = \varepsilon_c$
z	axial distance in streamwise direction from centre of seal clearance
Γ_c	ratio of discharge coefficients ($= C_{d,i} / C_{d,e}$)
ΔC_p	external pressure coefficient ($= \Delta p / 0.5 \rho \Omega^2 b^2$)
Δp	peak-to-trough pressure difference in annulus
	($= p_{2,max} - p_{2,min}$)
ε	sealing effectiveness ($= C_{w,o} / C_{w,e} = \Phi_o / \Phi_e$)
ε_c	concentration effectiveness
ε_p	pressure effectiveness
$\hat{\varepsilon}_p$	value of ε_p equal to ε_c
$\zeta(x)$	similarity parameter
θ	normalized angular coordinate between vanes
μ	dynamic viscosity
ρ	density
Φ_o	nondimensional sealing parameter
	($= C_{w,o} / 2\pi G_c Re_\phi$)
Φ_{min}	minimum value of Φ_o to seal wheel-space
$\chi(x)$	similarity parameter
Ω	angular speed of rotating disc

Subscripts

A	location A on vane platform
a	annulus
ax	axial
e	egress
EI	externally-induced ingress
i	ingress
max	maximum
min	minimum
o	sealing flow
rad	radial
s	stator surface
1,2	locations in wheel-space and annulus

Superscript

| *	value when $\Phi_o = 0$

1. Introduction

Fig. 1 shows a typical turbine stage and rim seal, where sealing air from the compressor is used to prevent or reduce the ingress (or ingestion) of hot mainstream gas into the wheel-space between the rotating turbine disc and the adjacent stationary casing. The sealing flow rate – and consequently the ingress of hot gas through the rim seal – depends on the available pressure drop between the compressor and turbine.

The stationary vanes and rotating blades create an unsteady three-dimensional distribution of pressure in the mainstream annulus near the seal clearance. Under these conditions, externally-induced (EI) ingress can occur, where the amount of ingress is strongly related to the time-average peak-to-trough pressure difference near the seal clearance. Ingress of hot gas occurs in those

2

circumferential regions of the clearance where the pressure in the annulus is higher than that in the wheel-space, and egress of the sealing air occurs in those regions where it is lower.

In experimental rigs, the sealing effectiveness of a rim seal can be readily and accurately determined from concentration measurements of a tracer gas (usually CO_2). Although pressure measurements can also be used to determine the sealing effectiveness, they are, in effect, proxy measurements, and the effectiveness determined in this way is strongly affected by the locations where the pressures are measured. The symbols ε_c and ε_p are used here to denote the sealing effectiveness determined from concentration and pressure measurements respectively, and in general $\varepsilon_c \neq \varepsilon_p$.

So-called orifice models can be used to relate the amount of ingress to the pressure difference across the rim seal but, to incorporate these models into design codes, the designer needs to know where in the turbine the pressures should be determined. More broadly, it is necessary to understand the relationship between ε_c and ε_p if the concentration measurements obtained from experimental rigs are to be used in the engine design methods.
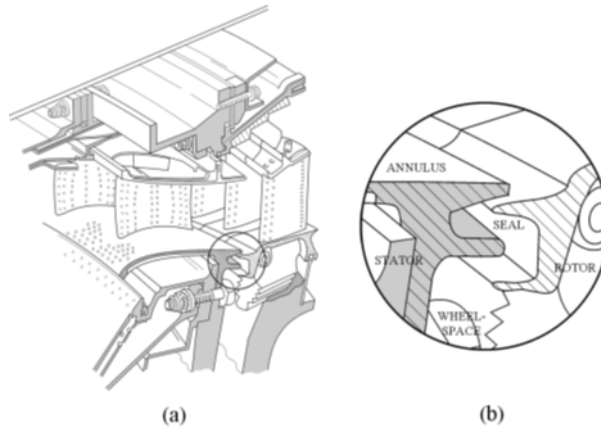
Fig. 1: (a) Typical high-pressure gas-turbine stage;
(b) detail of rim seal

In this paper a theoretical model is developed to enable the 'correct' value of ε_p to be determined from pressure measurements made at any arbitrary location (referred to as location A) on the vane platform, upstream of the seal clearance in a rig or engine. The model is based on a previously-published orifice model [1-2] and on the hypothesis that there is a unique location, referred to as the *sweet spot*, where the pressure distribution on the vane platform would ensure that $\varepsilon_c = \varepsilon_p$ for all sealing flow rates. Pressure and concentration measurements in a rotating-disc rig are used to validate the theoretical model and to determine values of ε_c and ε_p. This is principally an experimental and theoretical modelling paper but supporting computational fluid dynamics (CFD) is used to compute the location of the sweet spot.

A brief review of externally-induced ingress relevant to the present study is presented in Section 2. The experimental rig and instrumentation are described in Section 3. Section 4 discusses the development of the theoretical model and the computation of the location of the sweet spot. In Section 5, comparisons are made between the sealing effectiveness determined from the concentration measurements and the effectiveness calculated from the pressure measurements. Suggestions of how to use the model to estimate the sealing effectiveness in an engine are presented in Section 6. The principal conclusions are summarised in Section 7. An uncertainty analysis for the pressure measurements is shown in Appendix A, and an outline of the supporting CFD model is given in Appendix B.

2. Brief review of externally-induced (EI) ingress

The definition of symbols not defined below are given in the Nomenclature.

Computational fluid dynamics (CFD) has been used with some success to compute ingress and the reader is referred to Wang *et al.* [3] who provide a review of the recent CFD research. Although CFD is possible, predictions of the unsteady three-dimensional flows in both the annulus and wheel-space are computationally expensive and require significant expertise and insight. The papers discussed below are concerned principally with experimental measurements or theoretical modelling, which are at the heart of this paper.

Most experimental research on EI ingress has involved determining the value of the sealing flow rate necessary to prevent ingress or the sealing effectiveness when ingress occurs. Usually this has been accomplished by seeding the sealing air with CO_2 or another tracer gas and measuring the concentration on the stator. Recent examples include turbine-based rigs running close to engine-operating conditions, *e.g.* [4-6]; as well as simplified engine rigs specifically designed for detailed instrumentation access to a more benign environment, *e.g.* [7-8].

Experiments using pressure measurements to determine the minimum nondimensional sealant flow rate required to prevent ingress, were performed by Phadke and Owen [9] in a rig at Sussex University with an external annulus but *without* vanes or

GTP-14-1417   Sangan

blades. (A circumferential distribution of external pressure was created by gauze and honeycomb in the external annulus of the rig.) Using flow visualization, pressure and concentration measurements, they showed that the minimum sealing flow rate required to prevent EI ingress was proportional to the square-root of the peak-to-trough pressure difference in the annulus. Using rigs *with* external vanes and blades, Green and Turner [10] determined the sealing effectiveness using gas concentration and pressure measurements in a rig at Sussex University, but there was not good agreement between the values achieved from the two methods. Somewhat surprisingly, Green and Turner reported that the blades *reduced* ingress, compared to the case where only vanes were fitted. Conversely, Bohn *et al.* [11], using a rig at Aachen University, found that the blades *increased* ingress. Recent concentration measurements by Scobie *et al.* [12] in a rig at the University of Bath suggested that EI ingress was controlled principally by the pressure differences created by the vanes and that the blades in their rig appeared to have no significant effect.

Johnson *et al.* [13] used an orifice model to predict ingestion rates in the Aachen rig, using CFD to compute the unsteady pressure distribution in the annulus. A modified version of this model [14] was also successfully used to estimate the discharge coefficients for ingress and egress from experimental data from a rig at Arizona State University [15]. Chew *et al.* [16] had previously developed an alternative orifice model which successfully predicted discharge coefficients in the Sussex rig. Owen [1-2] recently created an orifice model (referred to here as the Bath orifice model) which uses variations of Bernoulli's equation with swirl, and relates the ingress and egress to the pressure drop across the seal. This model has been successfully applied to concentration measurements in the Bath rig.

Sangan *et al.* [17] used the Bath orifice model to derive the so-called *effectiveness equations* that express ε, the sealing effectiveness, in terms of Φ_o, the nondimensional sealing flow rate. For EI ingress:

$$\frac{\Phi_o}{\Phi_{min,EI}} = \frac{\varepsilon}{[1 + \Gamma_c^{-2/3}(1-\varepsilon)^{2/3}]^{3/2}} \qquad (2.1)$$

where

$$\Phi_o = \frac{C_{w,o}}{2\pi G_c \, \text{Re}_\phi} = \frac{U}{\Omega b} \qquad (2.2)$$

Γ_c is the ratio of the discharge coefficients for ingress and egress; $\Phi_{min,EI}$ is the minimum value of Φ_o, needed to prevent EI ingress; U is the bulk-average velocity of the sealing flow rate through the seal clearance; and Ωb is the tangential velocity of the rotor at the seal radius. Φ_o is therefore an inviscid parameter and ingress through the rim seal is essentially an inertial phenomenon. To use eq (2.1), it is necessary to determine Γ_c and Φ_{min} from correlations of the measured sealing effectiveness [18]; this is usually done using values of ε and Φ_o determined from concentration measurements.

Although the effectiveness equations require no knowledge of the pressure distribution in the annulus, this distribution is required if the experimental measurements and associated correlations are to be used in an engine design. For EI ingress, the orifice model [1] shows that

$$\Phi_{min,EI} = \frac{2}{3} C_{d,e} \Delta C_p^{1/2} \qquad (2.3)$$

where

$$\Delta C_p = \frac{\Delta p}{0.5 \rho \Omega^2 b^2} \qquad (2.4)$$

Δp is the peak-to-trough circumferential pressure difference in the annulus, and $C_{d,e}$ is the discharge coefficient for egress through the rim seal. Using CFD, Owen *et al.* [19] identified contours of non-dimensional pressure in the annulus where ΔC_p should be evaluated to ensure consistency between pressure- and concentration-based effectiveness. These contours suggested that the location of the sweet spot, referred to in Section 1, was close to the seal clearance.

## 3. Experimental measurements of sealing effectiveness

The test facility, which experimentally simulates hot gas ingress into the wheel-space of an axial turbine stage, is described extensively in Sangan *et al.* [17]. Only a brief overview of the research facility and its associated instrumentation is given below. To date, this rig has been used to determine sealing effectiveness based on *concentration*; in Section 5 the concentration effectiveness is compared with the effectiveness determined from *pressure* measurements.

Although a simple rig geometry and a generic rim seal are used for the results discussed here, complex seals representative of those used in engines can, and have been, tested in the rig.

3.1 Test rig

The test section of the facility, shown in Fig. 2, features a turbine stage with 32 vanes and 41 blades. The disc and blades were rotated by an electric motor. The blades were symmetric NACA 0018 aerofoils to avoid the necessity of a dynamometer to remove the unwanted power; the ratio of the leading-edge diameter to chord-length was 0.0984. The diameter of the disc was 380 mm and the height of the annulus was 10 mm.

The disc could be rotated at speeds up to 4000 rpm; this provided a maximum rotational Reynolds numbers, Re_ϕ (based on disc radius) up to 1.1×10^6. This value is typically an order-of-magnitude less than that found in gas turbines. However, for rotating flow the turbulent flow structure in the boundary layers is principally governed by the turbulent flow parameter, λ_T, and depends only weakly on Re_ϕ [20]. Hence the flow structure in the rig is considered to be representative of that found in the cooling systems of engines.
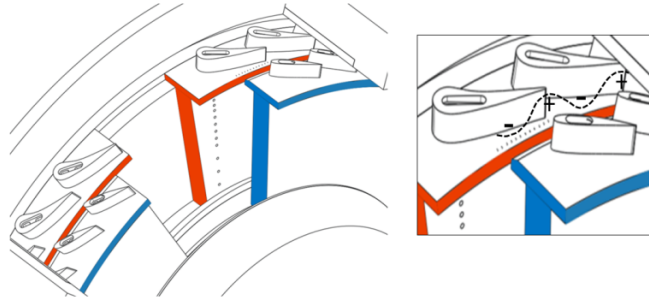
Fig. 2: Rig test section with inset highlighting the static pressure taps in the vane hub (location A) and typical pressure asymmetry in the annulus. (Red indicates the stationary disc and blue the rotating disc)

The vanes and blades in the annulus produced a flow structure representative of those found in engines, albeit at lower Reynolds and Mach numbers. The circumferential variation of static pressure was determined from 15 taps (each 0.5 mm diameter) arranged across one vane pitch, as illustrated in Fig. 2 (inset). These taps were located axially on the vane platform 2.5 mm downstream of the vane trailing edge and 2.5 mm upstream of the edge of the seal clearance. This axial location, which is referred to as *location A*, was where *Δp,* the peak-to-trough circumferential pressure difference, was determined. The pressures were measured using a Scanivalve system, which was connected to the taps with flexible plastic tubing, and data were averaged over four vane pitches. An uncertainty analysis of the pressure measurements is given in Appendix A.

Fig. 3 shows a typical circumferential variation of the pressure coefficient at location A, where

$$C_p = \frac{p_2 - \bar{p}_2}{1/2\rho\Omega^2 b^2} \qquad (3.1)$$

In this definition, θ is the normalised angular location between adjacent vanes, p_2 is the local static pressure at this location, and $\bar{p}_2$ is the mean pressure. Also shown in Fig. 3 is the comparison between the computed and pressure coefficients; the CFD model used for the computation is described in Appendix B. (As symmetrical blades were used in the rig, the time-average values of C_p determined by the Scanivalve system used here are unlikely to be the same as those found in an engine.)

In the wheel-space, a series of radial taps ($0.55 < r/b < 0.993$) were used to determine the distribution of static pressure and concentration along the stator. Sealing air was introduced into the wheel-space at a low radius ($r/b = 0.642$) through an inlet seal. In order to measure the degree of ingestion by means of concentration, the sealing flow was seeded to a 1% level with CO_2 tracer gas. The concentration measurements were made within a combined uncertainty of +/- 1.5% of the measured value; a detailed uncertainty analysis is presented by Sangan *et al.* [7].
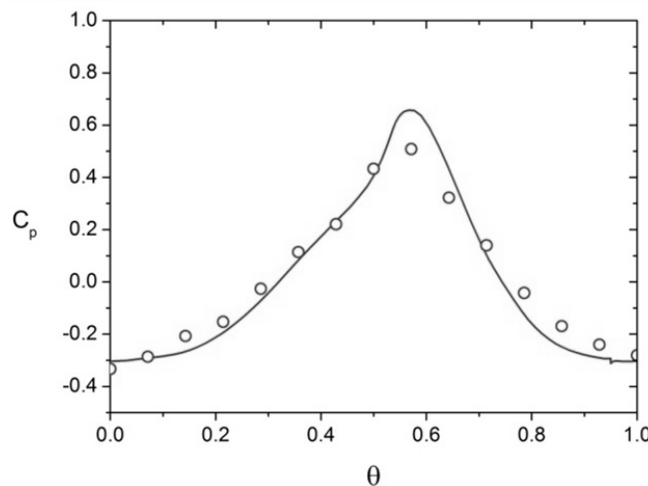
Fig. 3: Typical circumferential variation of pressure coefficient at location A in the annulus. $C_F = 0.538$, $Re_\phi = 8.17 \times 10^5$ and $\Phi_0 = 0$ (Symbols denote experimental measurements; curve shows computed variation.)

5

All data presented in this paper are for the *design condition*, with similar annulus velocity triangles at the three operating points listed in Table 1. At the design condition, the flow coefficient was $C_F = 0.538$ and the circumferential variation of C_p (Fig. 3) was shown to be independent of Re_ϕ. Measurements at off-design conditions $0 < C_F < 0.9$ are reported by Scobie *et al.* [12].

Parameter	Disc Speed (RPM)		
	2000	3000	3500
Re_ϕ	5.32 x 10^5	8.17 x 10^5	9.68 x 10^5
Re_w	2.86 x 10^5	4.40 x 10^5	5.21 x 10^5
C_F	0.538	0.538	0.538
M	0.225	0.339	0.398

Table 1: Parameters for EI experiments

3.2 Definition of sealing effectiveness

Concentration measurements were used to determine the *concentration effectiveness* ε_c. This is defined as

$$\varepsilon_c = \frac{c_s - c_a}{c_o - c_a} \qquad (3.2)$$

where the subscripts a, o and s respectively denote the air in the annulus, the sealing air at inlet, and at the surface of the stator. For the experiments conducted here, c_a and c_o were constants (approximately 1% and 0% respectively) and c_s varied with radius on the stator. In particular, $\varepsilon_c = 1$ when $c_s = c_o$ (zero ingress) and $\varepsilon_c = 0$ when $c_s = c_a$ (zero sealing flow).

3.3 Radial-clearance rim seal

A schematic diagram of the radial-clearance seal is shown in Fig. 4 with static dimensions. The seal-clearance ratio, $G_c = s_{c,ax} / b = 0.0105$ used in Eqs. (2.1) and (2.2) was based on the axial clearance $s_{c,ax} = 2.0$ mm.
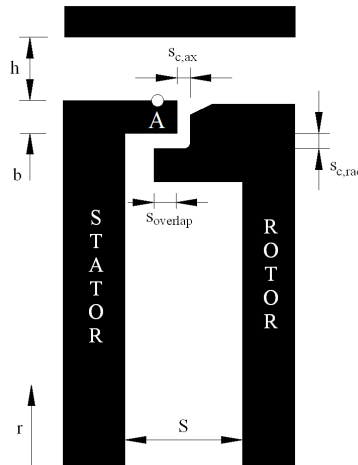
Fig. 4: Schematic of radial-clearance seal and annulus showing location A. Static dimensions in mm: h = 10; S = 20; $s_{c,ax}$ = 2.00; $s_{c,rad}$ = 1.28; $s_{overlap}$ = 1.86.

Figure 5 shows comparisons between the theoretical curve, eq (2.1), and the experimental values of ε_c based on the concentration measured on the stator at a non-dimensional radius $r/b = 0.958$. Φ_{min} and Γ_c were calculated from a statistical fit of the data [18], and their respective values were found to be 0.0915 and 1.32 for the radial-clearance seal. The experimental data, which are in good agreement with the theoretical curve, show that Re_ϕ, the rotational Reynolds number, has no significant effect on the results.

To date, this rig has been used to determine ε_c, the sealing effectiveness based on concentration. In Section 5, the data in Fig. 5 are compared with ε_p, the effectiveness determined from pressure measurements using the model discussed below.
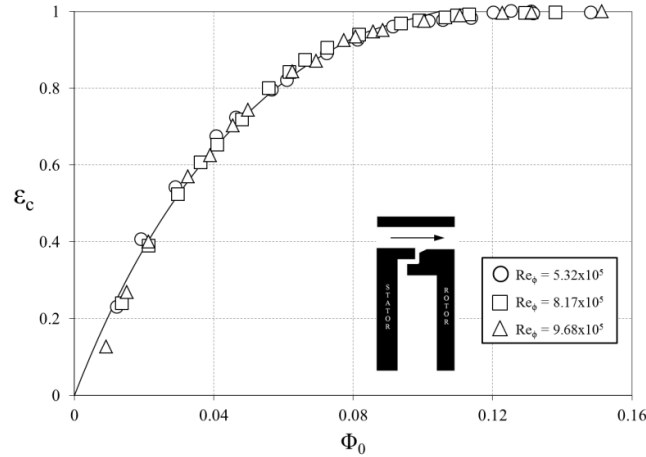
GTP-14-1417   Sangan

Fig. 5: Comparison between theoretical and measured values of ε_c for radial-clearance seal

4. Determination of sealing effectiveness from pressure measurements

As this section is concerned only with externally-induced (EI) ingress, the subscript EI is not used below.

4.1 Use of orifice model to calculate effectiveness

The Bath orifice model derived in [1-2] was based on pressures, and it was assumed that EI ingress is related to Δp, the peak-to-trough pressure difference in the annulus, where

$$\Delta p = p_{2,max} - p_{2,min} \qquad (4.1)$$

The sealing effectiveness in the model is related to g, the normalised pressure difference across the seal, where

$$g = \frac{p_1 - p_{2,min}}{\Delta p} \qquad (4.2)$$

The subscripts 1 and 2 refer to locations in the wheel-space and annulus respectively, *and these locations were not specified in the orifice model.*

By assuming a linear saw-tooth model for the circumferential distribution of pressure in the annulus, the orifice equations were solved in [2] to give

$$\frac{\Phi_o}{\Phi_{min}} = g^{3/2} - \Gamma_c (1-g)^{3/2} \qquad (4.3)$$

It was also shown from the orifice equations that

$$\varepsilon_p = 1 - \Gamma_c \left[\frac{1-g}{g} \right]^{3/2} \qquad (4.4)$$

As discussed above, ε_p is the sealing effectiveness based on pressure differences, and $\Gamma_c = C_{d,i}/C_{d,e}$ is the ratio of the discharge coefficients for ingress and egress through the seal clearance.

In practice, g (and therefore ε_p) depends on the sealing flow rate, *and it also depends on where the pressures are measured.* That is, $g = g(\Phi_o, x)$, where x is that axial location in the annulus where Δp is measured. At the sweet spot (where $x = \hat{x}$, $\varepsilon_p = \hat{\varepsilon}_p = \varepsilon_c$ and $g = \hat{g}$), eq (4.4) becomes

$$\hat{\varepsilon}_p = \varepsilon_c = 1 - \Gamma_c \left[\frac{1-\hat{g}}{\hat{g}} \right]^{3/2} \qquad (4.5)$$

Using eq (2.1), the effectiveness equation for ε_c, it follows from eq (4.5) that

$$\hat{g} = \frac{1}{1 + \Gamma_c^{-2/3} (1 - \varepsilon_c)^{2/3}} \qquad (4.6a)$$

Defining $\hat{g}^* = \hat{g}$ when $\Phi_o = 0$, and $\varepsilon_c = 0$, it follows from eq (4.6a) that

$$\hat{g}^* = \frac{\Gamma_c^{2/3}}{1 + \Gamma_c^{2/3}} \qquad (4.6b)$$

For the radial-clearance seal, $\Gamma_c = C_{d,i}/C_{d,e} = 1.32$ and so $\hat{g}^* = 0.546$.

It is shown below how $\hat{g}$ and $\hat{\varepsilon}_p$ can be determined from experimental measurements.

4.2 Determination of effectiveness from pressure measurements

7

In the model developed below, it is assumed that the *sweet spot*, where $g* = \hat{g}*$, can be found on the vane platform upstream of the clearance. This is consistent with the results of Owen *et al.* [19], who used steady 3D CFD based on the geometry of the Bath rig (but without blades and with an axial-clearance seal) to determine the sealing effectiveness.

In the annulus, $p_{2,min}$, $p_{2,max}$ and Δp depend on both Φ_o and x, where x is the nondimensional axial distance from the centre of the seal clearance; in the wheel-space, p_1 is invariant with x and depends only on Φ_o. To make these dependencies explicit, eq (4.2) is rewritten as

$$g(\Phi_o, x) = \frac{p_1(\Phi_o) - p_{2,min}(\Phi_o, x)}{\Delta p(\Phi_o, x)} \qquad (4.7a)$$

Similarly, at location A where the pressures are measured in the annulus, $x = x_A$ and

$$g(\Phi_o, x_A) = \frac{p_1(\Phi_o) - p_{2,min}(\Phi_o, x_A)}{\Delta p(\Phi_o, x_A)} \qquad (4.7b)$$

Eliminating p_1 from eqs (4.7a, b), it follows that

$$g(\Phi_o, x) = \frac{\Delta p(\Phi_o, x_A)}{\Delta p(\Phi_o, x)} g(\Phi_o, x_A) + \dots$$
$$\dots \frac{p_{2,min}(\Phi_o, x_A) - p_{2,min}(\Phi_o, x)}{\Delta p(\Phi_o, x)} \qquad (4.8)$$

Using a 'separation-of-variables' approach, it is assumed that
$$\Delta p(\Phi_o, x) = \zeta(x)\Delta p(\Phi_o, x_A) \qquad (4.9a)$$
and
$$[p_{2,min}(\Phi_o, x) - p_{2,min}(\Phi_o, x_A)] = \chi(x)\Delta p(\Phi_o, x_A) \quad (4.9b)$$
where $\zeta(x)$ and $\chi(x)$ are *similarity parameters* that depend on x but are assumed to be invariant with Φ_o. At location A, $\zeta(x_A) = 1$ and $\chi(x_A) = 0$.

Eq (4.8) can now be written as
$$g(\Phi_o, x) = \zeta(x)^{-1}[g(\Phi_o, x_A) - \chi(x)] \qquad (4.10)$$
Consequently, at the sweet spot where $x = \hat{x}$ and $g = \hat{g}$, eq (4.10) becomes

$$g(\Phi_o, \hat{x}) = \hat{g}(\Phi_o) = \zeta(\hat{x})^{-1}[g(\Phi_o, x_A) - \chi(\hat{x})] \quad (4.11a)$$
As $\zeta(\hat{x})$ and $\chi(\hat{x})$ are constants, eq (4.11a) can be expressed more simply as
$$\hat{g}(\Phi_o) = B\, g(\Phi_o, x_A) + C \qquad (4.11b)$$
where the constants B and C are given by

$$B = \zeta(\hat{x})^{-1} = \frac{\Delta p(\Phi_o, x_A)}{\Delta p(\Phi_o, \hat{x})} \qquad (4.12a)$$

$$C = -\frac{\chi(\hat{x})}{\zeta(\hat{x})} = -\frac{p_{2,min}(\Phi_o, \hat{x}) - p_{2,min}(\Phi_o, x_A)}{\Delta p(\Phi_o, \hat{x})} \qquad (4.12b)$$

As $x_A \to \hat{x}$ then $B \to 1$ and $C \to 0$.

Knowing $\hat{g}$ from eq (4.6a), the constants B and C in eq (4.11b) can be found from linear regression of $\hat{g}$ versus the measured values of $g(\Phi_o, x_A)$, as shown in Section 5.

The sealing effectiveness $\hat{\varepsilon}_p$, which in principle could be determined from pressure measurements at the sweet spot, can be calculated from (4.5) where

$$\hat{\varepsilon}_p(\Phi_o) = 1 - \Gamma_c \left[\frac{1 - C - Bg(\Phi_o, x_A)}{Bg(\Phi_o, x_A) + C}\right]^{3/2} \qquad (4.13)$$

As shown in Section 5, eq (4.13) ensures that the sealing effectiveness determined from pressure measurements is equivalent to that determined from concentration measurements.

4.3 Calculation of discharge coefficients at sweet spot

The discharge coefficient for egress, determined from measurements at location (A), can be calculated from eq (2.3) by

$$C_{d,e}(x_A) = \frac{3}{2}\frac{\Phi_{min}}{[\Delta C_p(x_A)]^{1/2}} \qquad (4.14)$$

This value depends on where the measurements are made, and the correct value to use is the one determined at the sweet spot, where

$$C_{d,e}(\hat{x}) = \frac{3}{2}\frac{\varPhi_{min}}{[\varDelta C_p(\hat{x})]^{1/2}} \qquad (4.15)$$

At the sweet spot, eq (4.12) shows that

$$\frac{\varDelta p(\varPhi_o, x_A)}{\varDelta p(\varPhi_o, \hat{x})} = B \qquad (4.16)$$

where, as described above, the constant B is found from linear regression of the pressure measurements. It follows from eq (4.16) that

$$\varDelta C_p(\hat{x}) = B^{-1}\varDelta C_p(x_A) \qquad (4.17)$$

Substitution in eq (4.15) gives

$$C_{d,e}(\hat{x}) = B^{1/2}C_{d,e}(x_A) \qquad (4.18a)$$

Similarly, for ingress,

$$C_{d,i}(\hat{x}) = B^{1/2}C_{d,i}(x_A) \qquad (4.18b)$$

As shown in Section 6, the discharge coefficients determined from measurements in an experimental rig could be used to compute the ingress through an engine rim seal.

4.4 Computation of location of sweet spot

In this section, CFD is used to support the experiments, which validate the theoretical model. The principal object of the CFD (details of which are given in Appendix B) was to determine the location of the sweet spot and to test the hypothesis that its location was invariant with the sealing flow rate.

Although, as shown above, the sealing effectiveness and the discharge coefficients can be calculated without knowing the location of the sweet spot, its location is needed if the experimental results are to be applied to an engine rim seal. As shown below, its location can be determined computationally using eqs (4.2) and (4.6).

Fig. 6 shows the computed axial distribution of $g(x)$, based on eq (4.2), for five values of $\varPhi_o/\varPhi_{min}$. The horizontal lines represent the five corresponding values of $\hat{g}$, which were calculated from eq (4.6) with the values of ε_c and $\varGamma_c$ determined from the concentration measurements. The intercept of these two curves occurs at the point where $g = \hat{g}$ and consequently where $x = \hat{x}$. The vertical line corresponds to the mean of the computed values of $\hat{x}$. (The values of p_1 were computed on the stator surface at $r/b = 0.958$, which is the location used for the experimental measurements discussed in Section 5.)
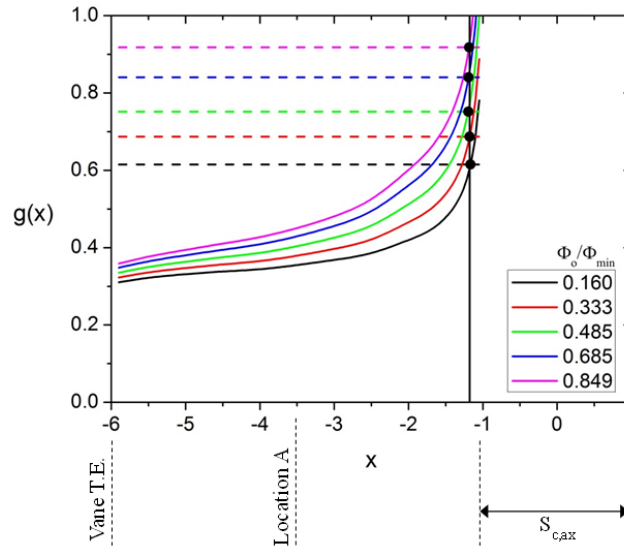
Fig. 6: Effect of $\varPhi_o/\varPhi_{min}$ on computed variation of $\hat{g}$ and g with x showing location of sweet spot. (Horizontal broken lines show values of $\hat{g}$; solid curve shows computed variation of $g(x)$; solid vertical line shows mean value of computed $\hat{x}$.)

Fig. 7 shows the computed values of $\hat{x}$ for the 22 values of $\varPhi_o/\varPhi_{min}$ used for the pressure measurements described in Section 5. The mean value of $\hat{x}$ for the radial-clearance seal was - 1.18, which is just 0.18 mm upstream of the seal clearance in the experimental rig. Although there is no reason to believe that this value will be the same for all seals, it is consistent with previous

9

GTP-14-1417   Sangan

computations for an axial-clearance seal in the same rig [see Sangan *et al.* 17]. The fact that there is no significant effect of the sealing flow rate on the computed values of $\hat{x}$ provides support for the assumption that $\hat{x}$ is invariant with Φ_o.
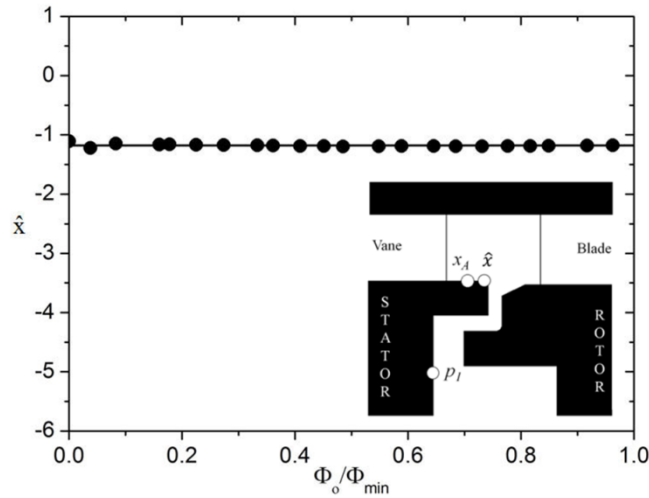

Fig. 7: Computed variation of $\hat{x}$ with $\Phi_o/\Phi_{\min}$. (Solid line shows mean value of $\hat{x}$, with its geometric position shown in relation to the seal clearance (inset))

5. Experimental measurements

The pressure measurements were obtained for the radial-clearance seal and Re_ϕ=8.17 x 10^5

Fig. 8 shows the measured variation of $g(x_A)$ with $\Phi_o/\Phi_{\min}$. As shown in Fig. 2, the static pressure on the surface of the stator, p_1, was measured at 14 different radial locations ($0.600 < r_1/b < 0.993$) in the wheel-space. For clarity, only five of these measurements are shown in the figure. It can be seen that there is no location of r_1/b that ensures that $g(x_A) = 1$ when $\Phi_o/\Phi_{\min} = 1$, which confirms the fact that location A cannot be the sweet spot, and consequently these uncorrected measurements cannot be used to determine the effectiveness.
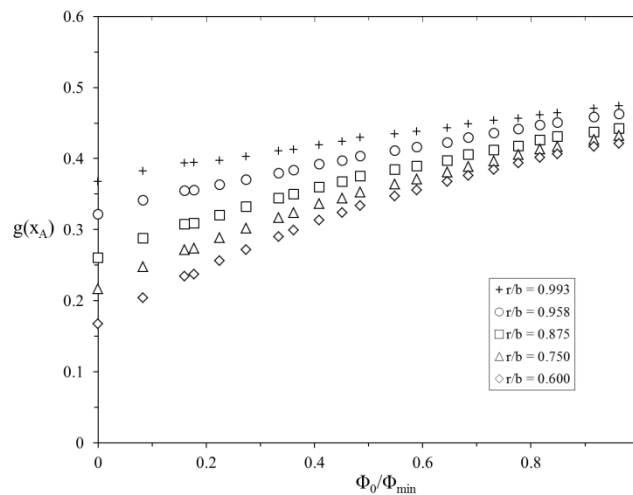

Fig. 8: Effect of r_1/b on measured variation of $g(x_A)$ with $\Phi_o/\Phi_{\min}$.

Although, in theory, the variation of $g(x_A)$ with $\Phi_o/\Phi_{\min}$ should be slightly nonlinear, the fact that the nonlinearity shown in Fig. 8 increases as r_1/b decreases is attributed to the swirl in the wheel-space. The swirl creates a nonlinear radial pressure gradient, and the difference between the pressures at the measurement radius r_1 and the seal radius b increases as r_1/b decreases.

There are two extremes to avoid in choosing a suitable location of r_1/b to measure p_1. As shown by Bohn *et al.* [21], if the radius is too close to the seal then the pressure in the wheel-space will be non-axisymmetric; if the radius is too small, the effects of swirl will be significant. (The effect of swirl on the radial distribution of pressure in the wheel-space of the rig used here is discussed in [22]). A value of $r_1/b = 0.958$ was chosen here as a compromise; this was also the radial location used to make the concentration measurements from which ε_c was determined.

10

Fig. 9 shows the variation of $g(x_A)$, the values of which were measured at $r_1/b = 0.958$, versus $\hat{g}$, calculated from eq (4.6a). Linear regression was used to determine the values of the constants, and it was found that $B = 3.07$ and $C = -0.472$. The standard deviation between the experimental values of $g(x_A)$ and the correlation was 0.012; in Appendix A, the uncertainty in the measured value of $g(x_A)$ was estimated to be ≤ 0.0077. These results support the assumptions made in deriving eq (4.12).
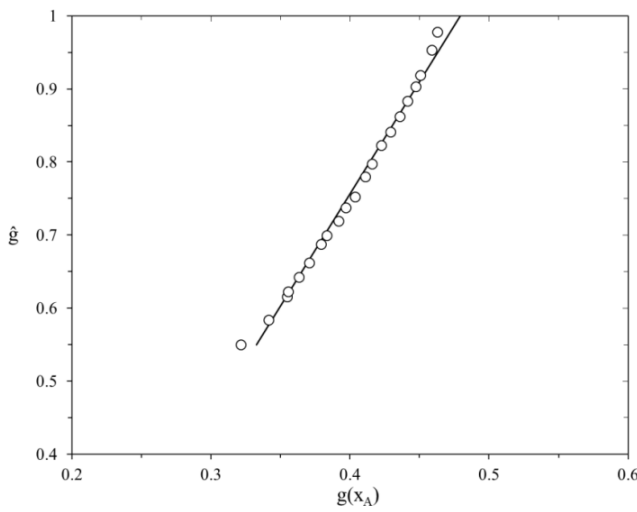
**Fig. 9: Variation of $\hat{g}$ with measured values of $g(x_A)$. (Solid line shows linear regression of data.)**

Fig. 10 shows the variation of $g(A)$ and $\hat{g}$ with Φ_o/Φ_{min}, where the curve for $\hat{g}$ was based on eq (4.6a) and the values of $g(x_A)$ are the same as those shown in Fig.9. For $\Phi_o = 0$, $\hat{g} = \hat{g}*$, and it follows from eq (4.6b) (with $\Gamma_c = 1.32$) that $\hat{g}* = 0.546$.
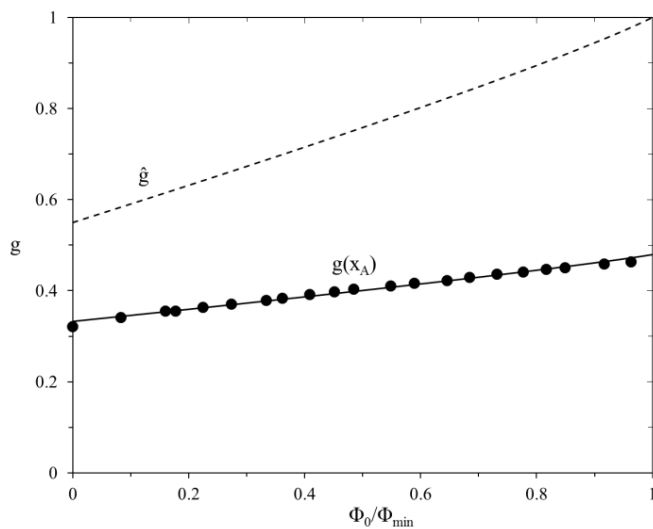
Fig. 10 Variation of $\hat{g}$ and $g(x_A)$ with Φ_o/Φ_{min}.

Fig. 11 shows the variation of sealing effectiveness with Φ_o/Φ_{min}. The values of ε_p were calculated from eq (4.13), using the values of B and C given above and the measured values of $g(x_A)$ shown in Fig. 10. The values of ε_c were obtained from the concentration measurements, and eq (2.1) was used to produce the effectiveness curve. The standard deviation between the calculated values of ε_p and the effectiveness curve was 0.017, and that between the measured values of ε_c and the curve was 0.019. (Note: these standard deviations were based on the differences between the individual calculated or measured values and the theoretical curve and not on the uncertainties calculated using Appendix A.)

These results give confidence in the theoretical model used in this paper.

GTP-14-1417   Sangan
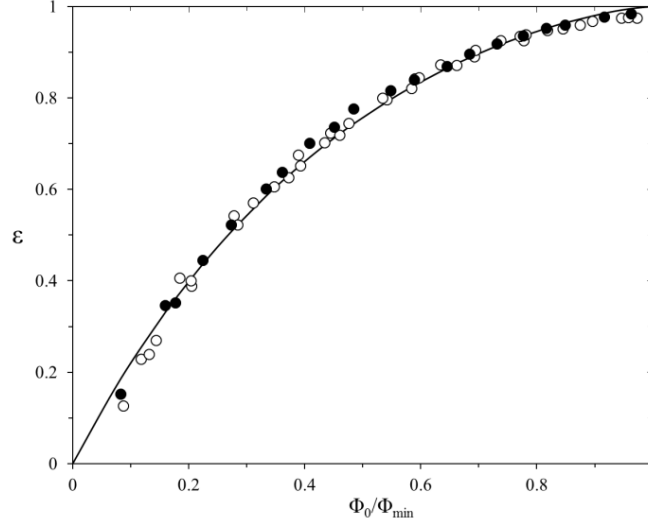
Fig. 11: Variation of sealing effectiveness with Φ_o/Φ_{min}. (Solid symbols denote values of ε_p from pressure measurements; open symbols denote values of ε_c from concentration measurements; solid curve is based on effectiveness equation.)

The values of $C_{d,e}$ and $C_{d,i}$ determined from the measurements of ΔC_p at location A were 0.177 and 0.239 respectively. Using eq (4.18) with B = 3.07, the values of $C_{d,e}$ and $C_{d,i}$ at the sweet spot are 0.310 and 0.419 respectively.

It is shown below how the model could be used by the engine designer.

6. Extrapolation of effectiveness data from rig to engine

In principle, orifice models provide a simple method of extrapolating the experimentally-measured effectiveness of a particular rim seal to a turbine with similar seal geometry. However, the conditions – particularly the Mach number and temperatures – in engines are usually significantly different from those in the experimental rig. Also, the design codes used for internal air systems usually estimate ingress from pressures rather than from the concentration measurements made in most rigs. Care and attention to mathematical consistency are needed if orifice models are used to extrapolate rig measurements to engine conditions. In particular, the 'correct' pressures must be used in the engine, and the theoretical model discussed above was developed to ensure that consistency.

The Mach number effect was considered by Teuber *et al.* [23] who showed, theoretically and computationally for the Bath rig, that the magnitude of ΔC_p increases as the Mach number increases. They showed that, by correcting ΔC_p and assuming that the discharge coefficients are unaffected by Mach number, the sealing effectiveness, ε_c, determined by concentration measurements in an experimental rig at one Mach number, could be used to compute the effectiveness in an engine at another Mach number. Their suggested correction for Φ_{min} is:

$$\frac{\Phi_{min,engine}}{\Phi_{min,rig}} = \left(\frac{\Delta C_{p,engine}}{\Delta C_{p,rig}} \right)^{1/2} \qquad (6.1)$$

where the ratio on the RHS of eq (6.1) is determined from the ratio of the Mach numbers. However, unless the location of the sweet spot is known, the effectiveness cannot be related to pressure differences in the engine. This makes the method of limited use to designers.

The location of the sweet spot in the engine has to be determined using CFD, as described in Section 4.4. (In the engine, unsteady CFD would be required to account for the turbine blades, which were not included in the steady CFD used in this paper.) The mean value of $\hat{x}$ could then be determined from computations made for a range of sealing flow rates. An approximate value could be found by computing $\hat{x}$ only for the case where the sealing flow rate is zero. For this case, $\hat{g} = \hat{g}^*$ where, as shown in Section 4.1,

$$\hat{g}^* = \frac{p_1^* - p_{2,min}^*(\hat{x})}{\Delta p^*(\hat{x})} = \frac{\Gamma_c^{2/3}}{1 + \Gamma_c^{2/3}} \qquad (6.2)$$

and Γ_c is known from the concentration measurements in the rig. The value of p_1^* could be evaluated at any convenient radial location in the wheel-space of the engine, bearing in mind the qualifications given in Section 5. The approximate value of $\hat{x}$ could then be found by computing $p_{2,min}^*(x)$ and $\Delta p^*(x)$ for different values of x, on the vane platform upstream of the seal clearance, until eq (6.3) is satisfied.

In the proposed method, it is assumed that the discharge coefficients at the sweet spot for the rim seal in the engine are equal to those at the sweet spot in the rig. As $C_{d,e,engine} = C_{d,e,rig} = C_{d,e}$, it follows that

12

$$\Phi_{min, engine} = \frac{2}{3} C_{d,e} \Delta C_{p,engine}^{1/2} \qquad (6.3)$$

where $\Delta C_{p,engine}$ is the time-average value determined at the sweet spot in the engine. As proposed by Teuber *et al.*, this relationship is assumed to apply for all Mach numbers.

For the case where $\Phi_o < \Phi_{min}$, it is necessary to calculate $\hat{g}$ *for any flow rate* by

$$\hat{g} = \frac{p_1 - p_{2,min}(\hat{x})}{\Delta p(\hat{x})} \qquad (6.4)$$

Knowing $\hat{g}$, the sealing effectiveness can be calculated from eq (4.5) where

$$\hat{\varepsilon}_p = 1 - \Gamma_c \left[\frac{1 - \hat{g}}{\hat{g}} \right]^{3/2} \qquad (6.5)$$

The uncertainties in $\hat{\varepsilon}_p$ depend on the uncertainties in $\hat{g}$, which, as shown in Appendix A, depend on the uncertainties in the pressures determined for the engine.

In conclusion, the principal assumptions in extrapolating from rig to engine are that the values of the discharge coefficients determined at the sweet spot for a particular seal in a rig are the same - regardless of the temperatures, pressures, densities and Mach numbers - as those at the sweet spot in an engine. To apply the model, the designer would need to use 3D unsteady CFD to determine the location of the sweet spot in the engine and the value of ΔC_p at this location. Knowing this value, the relevant equations could then be used to estimate the relationship between ingress and sealing flow rate for the engine.

The hypotheses made in the model cannot be verified using the existing Bath rig, which was designed to study the fundamental aspects of ingress. Facilities like the large HGIR rig described by Palafox *et al.* [4] and the Sussex rig used by Gentilhomme *et al.* [6] are more suitable for this purpose. Alternatively, it might be possible to use 3D unsteady CFD to test these hypotheses. The Bath experimental data and theoretical model provide a base for the prediction of ingress through turbine rim seals: it is up to the engine designers to build their procedures on this base.

7. Conclusions

The main object of this paper was to relate the sealing effectiveness determined from concentration measurements (ε_c) in an experimental rig to the effectiveness computed from pressure differences (ε_p) in an engine.

A theoretical model was developed to calculate the axial location (denoted by $\hat{x}$ and referred to as the 'sweet spot') where the pressures should be measured on the vane platform to ensure that $\varepsilon_p = \varepsilon_c$. The assumption was made that $\hat{x}$ should be invariant with Φ_o, the sealing flow parameter.

Concentration and pressure measurements were made on a single-stage turbine rig fitted with a radial-clearance rim seal. The concentration measurements were used, in conjunction with a previously published orifice model, to correlate the variation of ε_c with Φ_o for externally-induced ingress.

A nondimensional pressure difference (referred to as $g(x_A)$) was determined from measurements at an arbitrary location (location A) in the annulus. The pressure measurements showed that, as predicted by the model, $\hat{g}$, the nondimensional pressure difference at the sweet spot, varied linearly with $g(x_A)$ for $0 < \Phi_o/\Phi_{min} < 1$, where Φ_{min} is the minimum value of Φ_o needed to prevent ingress through the seal clearance.

Linear regression of $\hat{g}$ versus $g(x_A)$ was used to determine two constants, B and C, from which it was possible to calculate the variation of ε_p with Φ_o/Φ_{min}. The calculated values of ε_p were in good agreement with the measured values of ε_c and with the effectiveness equation derived from the orifice model.

Steady 3D CFD, based on the geometry of the experimental rig but without the rotating blades, was used to compute the value of $\hat{x}$ for $0 < \Phi_o/\Phi_{min} < 1$. These computations showed that, as assumed in the model, $\hat{x}$ was virtually invariant with Φ_o. As shown in a previously published paper, the computed value of $\hat{x}$ was found to be very close to the upstream edge of the seal clearance.

Using the model, $C_{d,e}(\hat{x})$ and $C_{d,i}(\hat{x})$, the discharge coefficients for egress and ingress at the sweet spot, could be related to $C_{d,e}(x_A)$ and $C_{d,i}(x_A)$, the discharge coefficients determined experimentally at location A in the rig.

It was shown how, in principle, the theoretical model could be used to determine the effectiveness for the rim seals in an engine. This would involve the use of CFD, together with the values of $C_{d,e}(\hat{x})$ and $C_{d,i}(\hat{x})$ determined from an experimental rig with a similar rim seal, to compute the sweet spot for the engine seal.

The Bath experimental data and theoretical model provide a base for the prediction of ingress through turbine rim seals: it is up to the engine designers to build their procedures on this base.

References

[1] Owen, J.M., 2011, "Prediction of Ingestion through Turbine Rim Seals---Part I: Rotationally Induced Ingress," ASME J. Turbomach., **133**(3), 031005-1 to 9.

[2] Owen, J.M., 2011, "Prediction of Ingestion through Turbine Rim Seals---Part II: Externally Induced and Combined Ingress," ASME J. Turbomach., **133**(3), 031006-1 to 9.

13

[3] Wang C.Z., Johnson B.V., Cloud D.F., Paolillo R.E., Vashist T.K., Roy R.P., 2006, "Rim Seal Ingestion Characteristics for Axial Gap Rim Seals in a Closely-spaced Turbine Stage from a Numerical Simulation," ASME Paper GT2006-90965.

[4] Palafox P., Ding Z., Bailey J., Vanduser T., Kirtley K., Moore K., Chupp R., 2013 "A New 1.5-stage Turbine Wheelspace Hot Gas Ingestion rig (HGIR) – Part I:Exprimental Test Vehicle, Measurement Capability and Baseline Results," ASME Paper GT2013-96020.

[5] Ding Z., Palafox P., Moore K., Chupp R., Kirtley K., 2013 "A New 1.5-stage Wheelspace Hot Gas Ingestion Rig (HGIR) – Part II: CFD Modeling and Validation," ASME Paper GT2013-96021.

[6] Gentilhomme, O., Hills, N. J., and Turner, A. B., 2003, "Measurement and Analysis of Ingestion through a Turbine Rim Seal," ASME J. Turbomach., **125**(3), pp. 505-512.

[7] Sangan, C. M., Pountney, O. J., Scobie, J. A., Wilson, M, Owen, J.M., and Lock, G.D., 2013 "Experimental Measurements of Ingestion through Turbine Rim Seals. Part 3: Single and Double Seals," ASME J. Turbomach., **135**(5), 051011-1 to 11.

[8] Zhou D.W., Roy R.P., Wang C.Z., Glahn J.A.. 2011, "Main Gas Ingestion in a Turbine Stage for Three Rim Cavity Configurations," ASME J. Turbomach., **133**(3), 031023 1 to 12.

[9] Phadke, U. P., and Owen, J. M., 1988, "Aerodynamic Aspects of the Sealing of Gas-Turbine Rotor-Stator Systems, Part 3: The Effect of Non-Axisymmetric External Flow on Seal Performance," Int. J. Heat Fluid Flow, **9**, pp. 113–117.

[10] Green, T., and Turner, A. B., 1994, "Ingestion into the Upstream Wheelspace of an Axial Turbine Stage," ASME J. Turbomach, **116**(2), pp. 327-332

[11] Bohn, D., Rudzinski, B., Sürken, N. and Gärtner, W., 2000, "Experimental and Numerical Investigation of the Influence of Rotor Blades on Hot Gas Ingestion into the Upstream Cavity of an Axial Turbine Stage," ASME Paper No. 00-GT-284

[12] Scobie, J.A., Sangan, C.M., Teuber, R., Pountney, O.J., Owen, J.M., Wilson, M., and Lock, G.D., 2013, "Experimental Measurements of Ingestion through Turbine Rim Seals. Part 4: Off-Design Conditions," ASME Paper GT2013-94147.

[13] Johnson, B. V., Jakoby, R., Bohn, D. E., and Cunat, D., 2006, "A Method for Estimating the Influence of Time-Dependent Vane and Blade Pressure Fields on Turbine Rim Seal Ingestion," ASME Paper GT2006-90853.

[14] Johnson, B. V. Wang, C.-Z., and Roy, P. R., 2008, "A Rim Seal Orifice Model with Two Cds and Effect of Swirl in Seals," ASME Paper No. GT2008-50650.

[15] Roy, R P, Zhou, D W, Ganesan, S, Wang, C-Z, Paolillo, R.E and Johnson, B. V., 2007, "The Flow Field and Main Gas Ingestion in a Rotor-Stator Cavity," ASME paper GT2007-27671.

[16] Chew, J. W., Green, T., and Turner, A. B., 1994, "Rim Sealing of Rotor-Stator Wheelspaces in the Presence of External Flow," ASME Paper No. 94-GT-126.

[17] Sangan, C. M., Pountney, O. J., Zhou, K., Wilson, M.,Owen, J. M., and Lock, G. D., 2013, "Experimental Measurements of Ingestion through Turbine Rim Seals. Part I: Externally-Induced Ingress," ASME J. Turbomach., **135**(2), 021012-1 to 10.

[18] Zhou, K., Wood, S. N., and Owen, J. M., 2013, "Statistical and Theoretical Models of Ingestion through Turbine Rim Seals," ASME J. Turbomach., 135(2), 021014-1 to 8.

[19] Owen, J. M., Zhou, K., Pountney, O. J., Wilson, M., and Lock, G. D., 2012, "Prediction of Ingress through Turbine Rim Seals---Part 1: Externally-Induced Ingress," ASME J. Turbomach., **134**(3), 031012-1 to 13.

[20] Childs, P.R.N., 2010, "*Rotating Flow*," Butterworth- Heinemann, Oxford.

[21] Bohn, D., Johann, E. and Kruger,U., 1995, "Experimental and Numerical Investigations of Aerodynamic Aspects of Hot Gas Ingestion in Rotor-Stator Systems with Superposed Cooling Mass Flow," ASME Paper 95-GT-143.

[22] Sangan, C.M., Lalwani, Y., Owen, J.M. and Lock, G.D., 2013, "Experimental Measurements of Ingestion through Turbine Rim Seals. Part 5: Fluid Dynamics of Wheel-space," ASME Paper GT2013-94148.

[23] Teuber, R., Wilson, M. Lock, G.D., Owen, J.M. Li, Y.S. Maltson, J.D., 2012, "Computational Extrapolation of Turbine Sealing Effectiveness from Test Rig to Engine Conditions," ASME Paper GT2012-68490.

Acknowledgements

Appendix A: Uncertainty in Pressure Measurements

From eq (4.2)

$$g = \frac{p_1 - p_{2,min}}{p_{2,max} - p_{2,min}} = \frac{X}{Y} \qquad (A1)$$

where $X = p_1 - p_{2,min}$ and $Y = p_{2,max} - p_{2,min}$. Hence

$$dg = \frac{\partial g}{\partial X} dX + \frac{\partial g}{\partial Y} dY \qquad (A2)$$

$$= \frac{dX}{Y} - X\frac{dY}{Y^2} \qquad (A3)$$

The magnitude of the relative uncertainty in g is then bounded by

$$\left|\frac{\delta_g}{g}\right| \leq \left|\frac{\delta_X}{X}\right| + \left|\frac{\delta_Y}{Y}\right| \qquad \text{(A4)}$$

where $\left|\delta_X\right| = \left|\delta_{p1}\right| + \left|\delta_{p2,min}\right|$ and $\left|\delta_Y\right| = \left|\delta_{p2,max}\right| + \left|\delta_{p2,min}\right|$, and $\delta_g, \delta_{p1}, \delta_{p2,min}, \delta_{p2,max}$ are the uncertainties in $g, p_1, p_{2,min}, p_{2,max}$ respectively. Hence,

$$\frac{\left|\delta_g\right|}{g} \leq \left\{ \frac{\left|\delta_{p1}\right| + \left|\delta_{p2,min}\right|}{p_1 - p_{2,min}} + \frac{\left|\delta_{p2,max}\right| + \left|\delta_{p2,min}\right|}{p_{2,max} - p_{2,min}} \right\} \quad \text{(A5)}$$

When the uncertainty is a percentage of the full-scale range, which was the case in the experiments, then $\left|\delta_{p1}\right| = \left|\delta_{p2,min}\right| = \left|\delta_{p2,max}\right| = \delta$, say, and eq (A5) simplifies to

$$\frac{\left|\delta_g\right|}{g} \leq \frac{2\delta}{p_{2,max} - p_{2,min}}(1 + g^{-1}) \quad \text{(A6)}$$

or

$$\left|\delta_g\right| \leq \frac{2\delta}{p_{2,max} - p_{2,min}}(1 + g) \qquad \text{(A7)}$$

The Druck PDCR 22 Scanivalve pressure transducers used in the experiments had a stated uncertainty of ±0.06% (Best Straight Line) across a range of 70 mbar, which implies that $\delta = 0.042$ mbar. In the experiments, $p_{2,max} - p_{2,min} \approx 16.3$ mbar, and $g(x_A) < 0.5$, so from eq (A7) $\left|\delta_g\right| \leq 0.0077$.

Appendix B: Computational model

The principal object of the CFD was to determine the location of the sweet spot and to test the hypothesis that its location was invariant with the sealing flow rate. Only a brief description of the CFD model is given here, and more details of the grid and rig geometry are given by Owen *et al.* [19].

As stated in Section 2, there is experimental evidence from the Bath rig to show that ingress is dominated by the circumferential difference in pressure generated by the vanes. (Scobie *at al.* [12] found that, except at extreme off-design conditions, the symmetrical turbine blades had little effect on ingress.) Consequently, the CFD model used here was based on the Bath rig *without the blades*; this allowed the use of a steady-flow code.

The commercial code CFD-13 was used, and the model geometry was based on the generic vanes and mainstream annulus of the Bath rig with a radial-clearance seal (see Section 3). The radius of the turbine disc was 195 mm and radial height of the vanes was 10mm. Only one vane-pitch of a ring of 32 vanes in the annulus was modelled, and cyclic symmetry was used at the circumferential faces of the 11.2°-sector model.

The flow rates and rotational speed corresponded to rotational and axial Reynolds numbers of $Re_\phi = 8.17 \times 10^5$ and $Re_w = 4.4 \times 10^5$. Sealing flow rates were in the range corresponding to $0 \leq \Phi_o \leq 0.0768$ for the radial-clearance seal. The fluid properties were based on experimental conditions at 21.9C and 3000 rpm. Radial equilibrium was assumed for the swirling air at the outlet boundary in the annulus, and the average pressure was taken to be atmospheric (1.01 bar).

Mesh sensitivity studies were carried out, as a result of which a mesh of 1.6 million cells was used in the model of the annulus and the wheel-space. The hexahedral mesh (produced by the ICEM software) was refined near wall surfaces so that the SST turbulence model of turbulence could be used with $y^+ \approx 1$ at most parts of rotor and stator discs.

Typical convergence level were less than 10^{-6} for normalized rms residuals, and total elapsed computing times of around five hours (using two 2.6 GHz processor cores) were needed.

GTP-14-1417   Sangan